VIP Lithium-Ion Batteries Very Important Paper

DOI: 10.1002/ange.201406719

Unravelling the Correlation between the Aspect Ratio of Nanotubular Structures and Their Electrochemical Performance To Achieve High-Rate and Long-Life Lithium-Ion Batteries**

Yuxin Tang, Yanyan Zhang, Jiyang Deng, Dianpeng Qi, Wan Ru Leow, Jiaqi Wei, Shengyan Yin, Zhili Dong, Rachid Yazami, Zhong Chen, and Xiaodong Chen**

Abstract: *The fundamental understanding of the relationship between the nanostructure of an electrode and its electrochemical performance is crucial for achieving high-performance lithium-ion batteries (LIBs). In this work, the relationship between the nanotubular aspect ratio and electrochemical performance of LIBs is elucidated for the first time. The stirring hydrothermal method was used to control the aspect ratio of viscous titanate nanotubes, which were used to fabricate additive-free TiO_2-based electrode materials. We found that the battery performance at high charging/discharging rates is dramatically boosted when the aspect ratio is increased, due to the optimization of electronic/ionic transport properties within the electrode materials. The proof-of-concept LIBs comprising nanotubes with an aspect ratio of 265 can retain more than 86 % of their initial capacity over 6000 cycles at a high rate of 30 C. Such devices with supercapacitor-like rate performance and battery-like capacity herald a new paradigm for energy storage systems.*

The provision of efficient electron and ion transport is a critical issue in developing electrode materials to achieve ultrafast rechargeable LIBs.[1] A prevalent strategy is to design nanostructured electrode materials with high conductivity and short path length,[2] since the diffusion time is proportional to the square of diffusion length and inversely proportional to diffusivity.[2d] Although different nanostructures have been developed to increase the cycle life and electrochemical performance of LIBs at high rates,[3] several features still limit the fundamental understanding of the relationship between LIB performance and nanostructured active materials,[4] owing to the use of polymeric binders[5] and conductive materials[3,6,7] in conventional battery construction. One such limitation is that the inhomogeneous blend of the additives and electroactive materials influences the diffusion paths of lithium ions and electrons in the electrode.[8] As a result, it is difficult to model and characterize the actual electrochemical reaction. Another limitation is that the additives, which normally account for the weight and volume increase of the electrode,[8] do not contribute to the actual battery storage performance but greatly alter the overall LIB performance. Therefore, a simple model of an additive-free electrode is required to precisely elucidate the correlation between the actual electrochemical performance and structural properties of the active materials.

In a conventional battery system, a polymer binder with the desired viscosity is required to mechanically secure the active materials and additives. However, if the active materials themselves are viscous enough to adhere well on the current collector, the binder is not needed in the battery system. Inspired by the hydrogel-like properties of one-dimensional (1D) fibrous structures,[9] we hypothesize that viscous 1D nanostructures may serve as electroactive materials to build battery cells without a binder. In addition, 1D nanostructures are advantageous in avoiding the use of conductive additives among multilevel nanostructures (Scheme S1), due to their direct and rapid ionic/electronic transport pathways and pronounced intrinsic/extrinsic conductivity.[2c,10] These reasons have strongly motivated us to develop elongated 1D nanostructures with high viscosity for application in additive-free electrode systems.

Herein, we use the stirring hydrothermal method (Figure 1 a) to prepare gel-like 1D TiO_2-based nanotubes (NTs) with different aspect ratios, a structural property that is strongly dependent on the viscosity of the precursor solution. We used such gel-like NTs as additive-free electrodes to fabricate LIBs (Scheme S1c) and discovered that the electronic/ionic transport properties of electrodes and LIBs performance can be modulated by the aspect ratio of the NTs. Impressively, LIBs with a remarkable high-rate and long-life performance were achieved with NTs having a large aspect ratio.

First we synthesized NTs with different aspect ratios. We selected TiO_2-based materials due to their excellent characteristics, such as safety, stability, and low volume expansion.[11] Based on the zero-shear viscosity theory (see the Supporting Information), it is known that solution viscosity (η_0) of a suspension is the sum of solvent viscosity (η_s) and a contribution from the suspended material [Eq. (1)].[12]

[*] Dr. Y. Tang,[+] Dr. Y. Zhang,[+] J. Deng, Dr. D. Qi, W. R. Leow, J. Wei, Dr. S. Yin, Prof. Z. Dong, Prof. R. Yazami, Prof. Z. Chen, Prof. X. Chen
School of Materials Science and Engineering
Nanyang Technological University
50 Nanyang Avenue, Singapore 639798 (Singapore)
E-mail: aszchen@ntu.edu.sg
chenxd@ntu.edu.sg
Homepage: http://www.ntu.edu.sg/home/chenxd/

[+] These authors contributed equally to this work.

[**] This work was supported by the Singapore National Research Foundation (NRF-RF2009-04 and CRETAE Programme on Nanomaterials for Energy and Water management).

Supporting information for this article is available on the WWW under http://dx.doi.org/10.1002/anie.201406719.

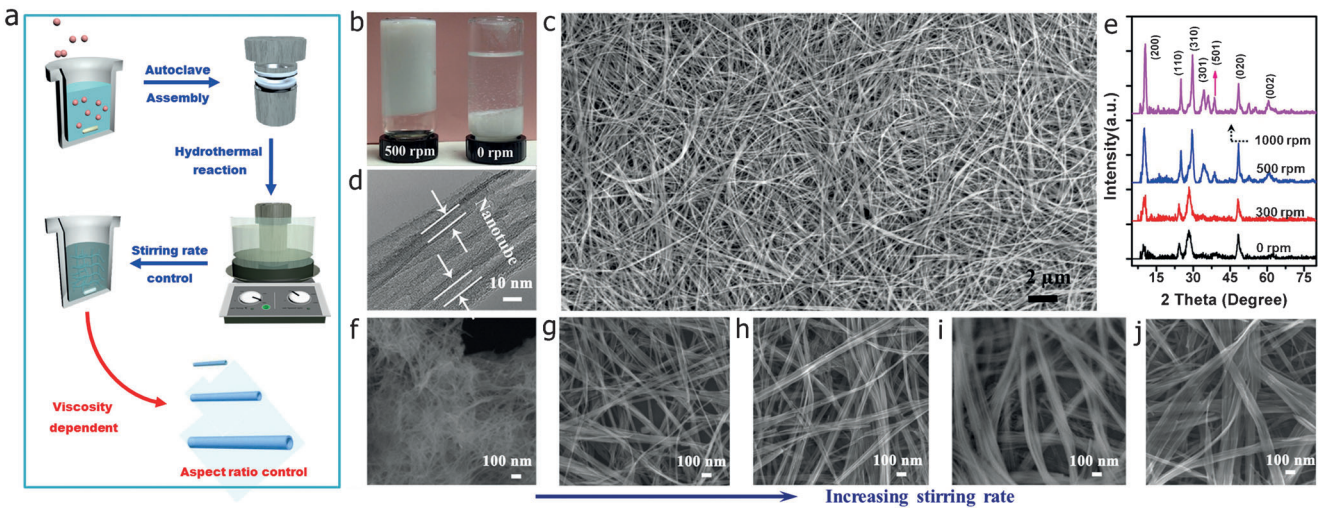

Figure 1. Fabrication and characterization of titanate NTs with different aspect ratios. a) Fabrication scheme. b) Digital photos of titanate solutions obtained by the stirring hydrothermal method at 500 (left) and 0 rpm (right) after sedimentation. c) FESEM images of titanate NTs obtained at 500 rpm. d) TEM image of (c), the arrow indicates a nanotubular structure. e) XRD patterns of the products synthesized at different stirring speeds. f–j) FESEM images of the titanate NTs obtained by hydrothermal reaction at 130 °C for 24 h in at stirring rates of 0, 300, 400, 500, and 1000 rpm, respectively.

$$\eta_0 = \eta_s + \frac{2}{15}\nu\zeta_r \tag{1}$$

Here ν is the number of NTs per unit volume and ζ_r is the rational friction coefficient. In the traditional hydrothermal reaction for the preparation of titanate NTs,[13] a low-viscosity solution is formed due to the settling of short titanate NTs and the weak interactions among them. To achieve a high-viscosity solution of NTs for the preparation of additive-free electrode LIBs, it is essential to increase the concentration of suspended NTs (ν) and strengthen their interactions (ζ_r). In this regard, the controlled concentration of the TiO_2 precursor in solution and the formation of a cross-linking network of extended nanotubular structures are desired. We recently proved that longer NTs could be prepared by a mechanical force-driven stirring process.[14] Therefore, it is hypothesized that the NT aspect ratio can be controlled by tuning the solution viscosity through the "polymerization" of the starting material, which is strongly dependent on the stirring rate (Figure 1a and the Experimental Section in Supporting Information).

As expected, titanate NTs with gel-like properties and a high aspect ratio could be prepared by controlling the stirring rates (Figure 1a and Scheme S2). As shown in Figure 1b, a gel-like titanate mixture is obtained at 500 rpm while a laminating solution is formed at 0 rpm. For simplification, the NTs obtained will be denoted as "NT-n", in which n refers to the stirring rate. Figure 1c reveals that the synthesized NT-500 is continuous and tens of micrometers in length. In addition, the multiwalled nanotubular structure with hollow interior seen in the NT-500 sample (Figure 1d) can also be observed for the other NTs prepared at different stirring rates (Figure S1), and the resultant NTs are confirmed to be crystalline titanate phase[15] (Figure 1e). It is noted that the diameter and length of the NTs (Figure 1f–j, Figure S1) can be fine-tuned by adjusting the stirring rate; the aspect ratios of the resultant NTs, defined as the length divided by the diameter, are summarized in Table S1. The increase in tube dimensions (Figure 2a) and the aspect ratio of the NTs is due to the gradually improved mass transport upon mechanical stirring inside the autoclave. The aspect ratio of NTs (Table S1) and the viscosity of the resultant solution (Figure 2b) are increased at stirring rates up to 500 rpm, after which a decrease is observed at 1000 rpm (detailed analysis in the Supporting Information). However, a linear correlation between the viscosity of the resultant solution and the square of the aspect ratio (δ) of the nanotube structure is observed (Figure 2c), and it agrees well with zero-shear viscosity theory [Eq. (2)].[12]

$$\eta_0 \propto \alpha\delta^2 \tag{2}$$

This relation is derived from Equation (1) and α is a correction factor. Equation (2) provides insight to control the growth of the NTs with different aspect ratios by tuning the solution viscosity.

Next, we prepared the additive-free battery cells from these titanate NTs by the detailed process shown in the Supporting Information. Despite the phase transformation (Figure S2) induced by vacuum annealing, the hollow nanotube morphology is well maintained, and the diameter and length of NTs do not exhibit any obvious changes (Figure S3). Thus, the aspect ratio of the NTs after annealing is maintained. Although the surface areas (S) of the various NTs show large differences before annealing, the differences are minimized and the average surface area is $132 \pm 28\ m^2 g^{-1}$ (Figure 2d) after annealing (see note in the Supporting Information). Through the geometrical calculation of the nanotube characteristics (see note in Supporting Information), the thickness (h) of the nanotube can be derived from Equation (3).

$$S = 2/\rho h \tag{3}$$

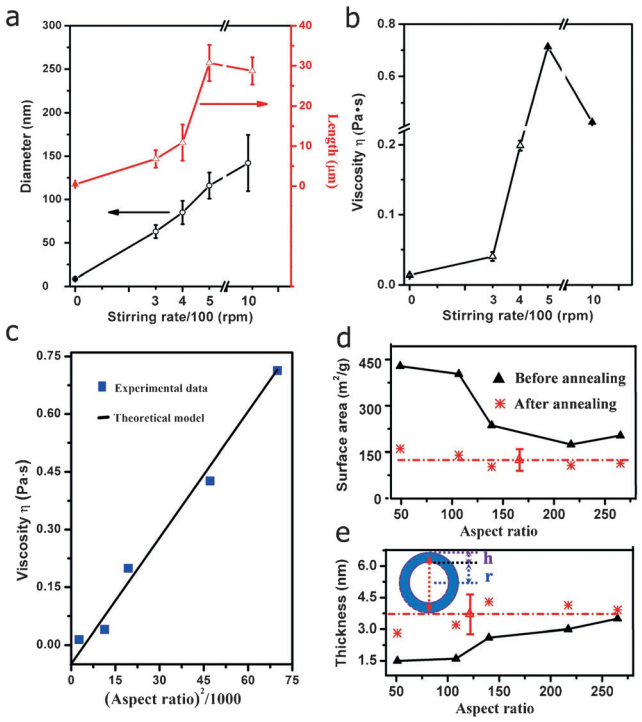

Figure 2. Correlation of the stirring rate on the geometric parameters, solution viscosity, surface area, and aspect ratio of NTs. The effects of stirring rate on a) the length and diameter of NTs and b) the viscosity of the resultant NT solution before thermal treatment. c) The relationship between the NT aspect ratio and the corresponding solution viscosity. d, e) The relationship between the aspect ratio and surface area and average tube thickness before (black) and after (red) annealing; the red dotted lines represent the mean surface area and tube thickness after annealing, and the error bars show the standard deviation. The inset in (e) is a schematic illustration of the nanotube cross-section (h: tube thickness, r: inner tube diameter).

Here ρ refers to the density of titania. From Equation (3), it is evident that the surface area is dependent on the NT wall thickness and not on the NT length. Therefore, the decrease in the surface area and pore volume (Figures S4 and S5) of the annealed TiO_2 NTs is due to the increase of NT thickness. After thermal treatment, the average thickness of various TiO_2 NTs falls within a narrow range of 3.7 ± 0.8 nm (Figure 2e). The minor differences both in the surface areas and the thicknesses of NTs are very profitable for clarifying the correlation of the aspect ratio with the LIB performance.

As an example of the application in additive-free LIBs, we tested the electrochemical performance of the TiO_2 NT-500 electrode (Figure S6). The high discharge and charge capacities of about 273 and 225 mAh g^{-1}, respectively, were exhibited for the first cycle. The capacity loss can be rationalized by the formation of solid–electrolyte interface layers.[16] In the subsequent cycles, a high Coulombic efficiency above 96.9% is obtained. The rate performance of the NT-500 electrode decreases slowly with discharge capacity from 222 to 116 mAh g^{-1}, while the current rate increases from *C*/5 to 30 *C* respectively. More importantly, the electrode shows stable cycling performance at high rates over extended time (Figure S7), indicating that the obtained TiO_2 NT electrode is suitable for application in additive-free LIBs.

Based on the same configuration, we systematically studied the correlation between the aspect ratio of the NTs and the electrodes' electrochemical performance (Figure 3). It reveals that the discharge capacity increases with increasing stirring rate, indicating that the NTs with a higher aspect ratio display better electrochemical performance (Figure 3a,b). At a low rate of *C*/5, these samples show very similar discharge capacities since the diffusion time is long enough for Li^+ ion insertion. With an increase in the discharging rate, the difference in discharge capacities between the electrodes prepared from high- and low-aspect-ratio NTs becomes more obvious. For example, at a high rate of 30 *C*, capacities of 1.4 and 116 mAh g^{-1} were delivered by NT-0 and NT-500, respectively. For electrodes prepared from high-aspect-ratio TiO_2 NTs, the rate capacity drops slightly with increasing discharge rate, which indicates that they can tolerate ultrafast extraction/insertion of Li^+ ions at high rates (Figure 3b).

Now, the fundamental question is: what is the key factor controlling the electrochemical performance of 1D NTs and how does it affect the battery performance? We first identified surface area as a potential key factor since the general perception is that electrode materials with higher surface areas normally possesses better electrochemical performance.[17] However, this characteristic does not explain all of our observations. Another possibility is that the TiO_2 phase (Figure S2) obtained from the thermal treatment of titanate may influence the battery performance since the TiO_2(B) phase has a higher theoretical capacity[11c,16] than anatase TiO_2. However, NT-1000 was observed to have lower capacity (108 mAh g^{-1}) than NT-500 (116 mAh g^{-1}) at 30 *C* (Figure 3a), despite some TiO_2(B) phase in the electrode. More importantly, the capacity is observed to increase gradually with the increase of the aspect ratio from NT-0 (1.4 mAh g^{-1}) to NT-300 (84 mAh g^{-1}) and NT-400 (92 mAh g^{-1}) of pure anatase phase, as well as from NT-400 to NT-500. Therefore, it is believed that the gradual enhancement of the battery performance is mainly due to the larger aspect ratio rather than phase difference or surface area of the nanotubes.

This discovery begs the question: how does the NT aspect ratio influence electron/ion transport, and in turn affect LIB performance. It should be noted that the calculated average thickness of TiO_2 NTs is less than 10 nm (Figure 2e). According to Equation (4), the characteristic diffusion time (t) is far less than 1 s along the axial direction and more than 10^4 s along the radial direction with 1 μm length.[2d]

$$t \approx \frac{l^2}{\alpha} \tag{4}$$

Here l represents diffusion length and α is ion diffusivity (α is around 10^{-12} cm^2 s[18] for TiO_2). Thus, the Li^+ ion diffusion pathway traverses along the radial direction of the nanotube (Figure 3c), and the thin tubes facilitate rapid ion/electron transport at high rates. Previous work[19] showed that Li^+ diffusion in anatase is not very anisotropic; thus Li^+ ions can diffuse along different planes in anatase despite their difference in diffusion energy barriers.[20] For our samples, the thermally stable {101} plane of anatase TiO_2 is observed

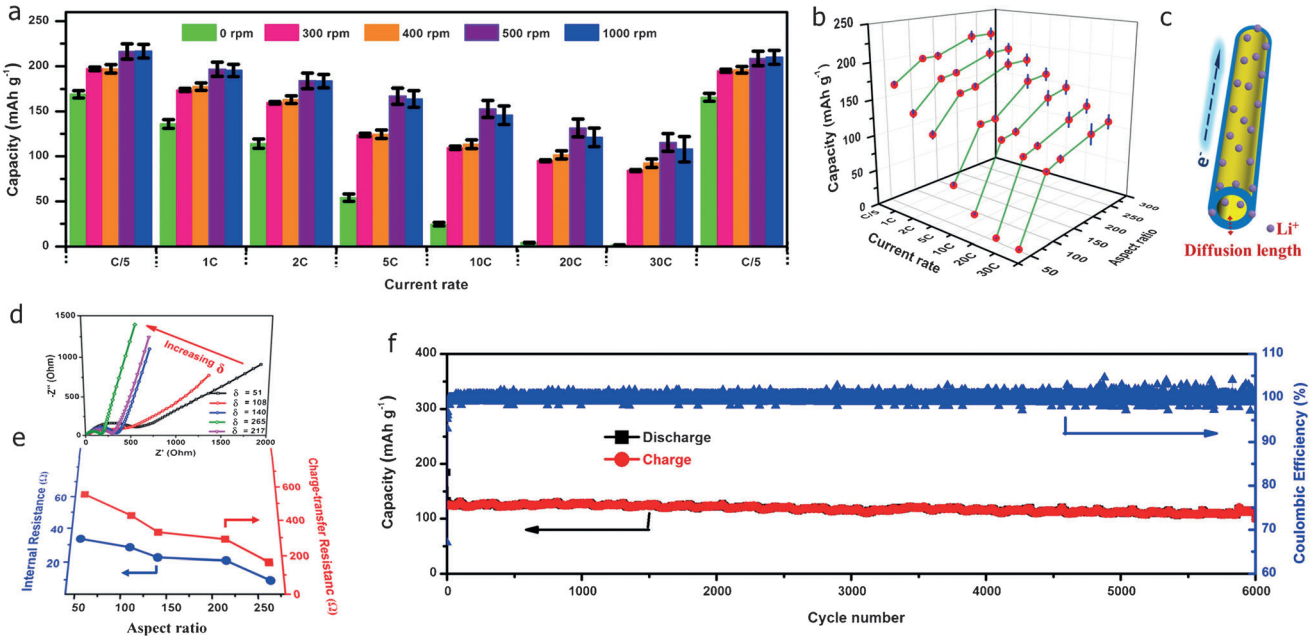

Figure 3. Electrochemical performance of the TiO_2 NT electrodes with different aspect ratios. a) Statistical study of the rate performance conducted at each current density based on the discharge capacity of final cycle with ten cells as one batch. b) Correlation between the aspect ratio and the capacity of different NTs at various discharging rates (1 C = 168 mA g^{-1}). c) Scheme of the electron and Li^+ transport pathways. d) Nyquist plots of the NT electrodes; Z' and Z'' represent the real and virtual parts of the complex-value impedance, respectively. e) Correlation between the aspect ratio and internal resistance and charge-transfer resistance of the as-prepared electrodes. f) Long-term cycling performance of NT-500 electrodes at a high rate of 30 *C*, showing the reversible capacity value of 114 mAh g^{-1} after 6000 cycles with a Coulombic efficiency around 100%.

(Figure S3) after annealing. According to the model (Figure S8) of the Li^+ ion transport pathway, Li^+ ions can easily diffuse into the {101} plane along the ⟨111⟩ direction as the TiO_6 octahedral is arranged in this direction, leaving an empty zigzag channel in three-dimensional networks.[21] The model in Figure S8 also indicates the other possible Li^+ ion diffusion pathways in other directions through the void channel. Thus, Li^+ ions can rapidly diffuse within the thin tube thickness of the TiO_2 NTs in various directions, resulting in the highly reversible capacity at high rate of 30 *C*. However, a huge difference in capacity is observed between nanostructures having different aspect ratios, with the capacity drop being particularly serious for the low-aspect-ratio samples at high discharging rates (Figure 3b). This leads us to hypothesize that the electron/ion transport in electrode and electrolyte should be a limiting factor accountable for this difference.

To prove this, the ionic and electronic resistance of NT electrodes was tested (Figure 3d,e). We found that each Nyquist plot consists of a high- to medium-frequency semicircle and a linear Warburg region for all the electrodes. The high-frequency region is characteristic of internal resistance, which consists of the resistance of the electrode/electrolyte interface, the separator, and the electrical contacts. The internal resistance decreases with the increase in aspect ratio, which indicates that high-aspect-ratio NTs possess a minor interface resistance, which facilitates the efficient electronic transport along the axial direction (Figure 3c). The medium-frequency region is associated with the charge-transfer resistance related to Li^+ ion interfacial transfer, coupled with a double-layer capacitance at the interface. It can be clearly seen that the charge-transfer resistance also decreases with aspect ratio, indicating the decreased ionic resistance and enhanced kinetics for high-aspect-ratio NTs. This is a result of their penetrable structure which is favorable for the flow and exchange of electrolytes (Figure 1g–j). Overall, the short Li^+ ion diffusion length and low internal/charge-transfer resistance have enabled us to prepare a long-life LIB with supercapacitor-like rate performance and battery-like capacity from large-aspect-ratio NTs.

Finally, as a proof-of-concept, LIBs comprising additive-free TiO_2 NTs with a large aspect ratio of 265 exhibit excellent stability over 6000 cycles at an ultrahigh rate of 30 *C* while retaining 86% of their initial capacity (133 mAh g^{-1}, Figure 3f), and the nanotubular morphology is well retained after cycling over extended times (Figure S9). It is worth noting that the our material exhibits the best performance for additive-free TiO_2-based LIBs[22] so far (Table S2), and its is comparable to that of the highest reported value for pure TiO_2 electrodes[11d,23] and its composite electrodes with additives.[16b,24]

In summary, the correlation between the NT aspect ratio and the battery performance has been revealed for the first time in an additive-free electrode system. We have discovered that the NT aspect ratio determines the electron/ion transport properties of electrode materials, and the high-rate performance of LIBs is significantly enhanced at higher NT aspect ratios. Impressively, the outstanding LIBs based on high-aspect-ratio TiO_2 NTs demonstrate ultrahigh rates and long lifetimes over 6000 charge/discharge cycles, attributed to high electronic/ionic conductivity and short lithium diffusion

length. This fundamental understanding should be extremely useful in the development of efficient energy devices by exploiting the properties of unique nanostructures.

Received: July 6, 2014
Published online: August 28, 2014

Keywords: aspect ratio · lithium-ion batteries · nanotubes · TiO_2

[1] a) P. S. Herle, B. Ellis, N. Coombs, L. F. Nazar, *Nat. Mater.* **2004**, *3*, 147; b) P. Simon, Y. Gogotsi, B. Dunn, *Science* **2014**, *343*, 1210.

[2] a) Y. S. Hu, X. Liu, J. O. Muller, R. Schlogl, J. Maier, D. S. Su, *Angew. Chem. Int. Ed.* **2009**, *48*, 210; *Angew. Chem.* **2009**, *121*, 216; b) J. M. Feckl, K. Fominykh, M. Döblinger, D. Fattakhova-Rohlfing, T. Bein, *Angew. Chem. Int. Ed.* **2012**, *51*, 7459; *Angew. Chem.* **2012**, *124*, 7577; c) H. Wu, G. Chan, J. W. Choi, I. Ryu, Y. Yao, M. T. McDowell, S. W. Lee, A. Jackson, Y. Yang, L. B. Hu, Y. Cui, *Nat. Nanotechnol.* **2012**, *7*, 309; d) H. G. Zhang, X. D. Yu, P. V. Braun, *Nat. Nanotechnol.* **2011**, *6*, 277.

[3] a) J. M. Tarascon, M. Armand, *Nature* **2001**, *414*, 359; b) S. Xin, Y. G. Guo, L. J. Wan, *Acc. Chem. Res.* **2012**, *45*, 1759; c) A. S. Aricò, P. Bruce, B. Scrosati, J. M. Tarascon, W. Van Schalkwijk, *Nat. Mater.* **2005**, *4*, 366; d) B. Kang, G. Ceder, *Nature* **2009**, *458*, 190–193; e) A. Magasinski, P. Dixon, B. Hertzberg, A. Kvit, J. Ayala, G. Yushin, *Nat. Mater.* **2010**, *9*, 353; f) H. Jung, M. W. Jang, J. Hassoun, Y. Sun, B. Scrosati, *Nat. Commun.* **2011**, *2*, 516; g) N. Li, Z. Chen, W. Ren, F. Li, H.-M. Cheng, *Proc. Natl. Acad. Sci. USA* **2012**, *109*, 17360; h) J. Wang, N. Yang, H. Tang, Z. Dong, Q. Jin, M. Yang, D. Kisailus, H. Zhao, Z. Tang, D. Wang, *Angew. Chem. Int. Ed.* **2013**, *52*, 6417; *Angew. Chem.* **2013**, *125*, 6545.

[4] a) Q. Zhang, E. Uchaker, S. L. Candelaria, G. Cao, *Chem. Soc. Rev.* **2013**, *42*, 3127; b) A. L. M. Reddy, S. R. Gowda, M. M. Shaijumon, P. M. Ajayan, *Adv. Mater.* **2012**, *24*, 5045; c) J. Qian, X. Wu, Y. Cao, X. Ai, H. Yang, *Angew. Chem. Int. Ed.* **2013**, *52*, 4633; *Angew. Chem.* **2013**, *125*, 4731; d) H. K. Noh, H. S. Park, H. Y. Jeong, S. U. Lee, H. K. Song, *Angew. Chem. Int. Ed.* **2014**, *53*, 5059; *Angew. Chem.* **2014**, *126*, 5159; e) S. Xu, C. M. Hessel, H. Ren, R. Yu, Q. Jin, M. Yang, H. Zhao, D. Wang, *Energy Environ. Sci.* **2014**, *7*, 632; f) X. Lai, J. E. Halpert, D. Wang, *Energy Environ. Sci.* **2012**, *5*, 5604.

[5] a) I. Kovalenko, B. Zdyrko, A. Magasinski, B. Hertzberg, Z. Milicev, R. Burtovyy, I. Luzinov, G. Yushin, *Science* **2011**, *334*, 75; b) B. Koo, H. Kim, Y. Cho, K. T. Lee, N. S. Choi, J. Cho, *Angew. Chem. Int. Ed.* **2012**, *51*, 8762; *Angew. Chem.* **2012**, *124*, 8892.

[6] a) W. Li, F. Wang, S. S. Feng, J. X. Wang, Z. K. Sun, B. Li, Y. H. Li, J. P. Yang, A. A. Elzatahry, Y. Y. Xia, D. Y. Zhao, *J. Am. Chem. Soc.* **2013**, *135*, 18300; b) G. Jeong, J. G. Kim, M. S. Park, M. Seo, S. M. Hwang, Y. U. Kim, Y. J. Kim, J. H. Kim, S. X. Dou, *ACS Nano* **2014**, *8*, 2977; c) C. B. Zhu, X. K. Mu, P. A. van Aken, Y. Yu, J. Maier, *Angew. Chem. Int. Ed.* **2014**, *53*, 2152; *Angew. Chem.* **2014**, *126*, 2184; d) S. Lee, Y. Cho, H. K. Song, K. T. Lee, J. Cho, *Angew. Chem. Int. Ed.* **2012**, *51*, 8748; *Angew. Chem.* **2012**, *124*, 8878.

[7] a) S. Yang, X. Feng, K. Mullen, *Adv. Mater.* **2011**, *23*, 3575; b) S. Yang, Y. Sun, L. Chen, Y. Hernandez, X. Feng, K. Mullen, *Sci. Rep.* **2012**, *2*, 427; c) J. Pikul, H. Zhang, J. Cho, P. V. Braun, W. P. King, *Nat. Commun.* **2013**, *4*, 1732; d) J. Lin, A. R. O. Raji, K. W. Nan, Z. W. Peng, Z. Yan, E. Samuel, D. Natelson, J. M. Tour, *Adv. Funct. Mater.* **2014**, *24*, 2044; e) Z. Wu, W. Ren, L. Wen, L. Gao, J. Zhao, Z. Chen, G. Zhou, F. Li, H. Cheng, *ACS Nano* **2010**, *4*, 3187; f) H. Wang, L. Cui, Y. Yang, H. Casalongue, J. Robinson, Y. Liang, Y. Cui, H. Dai, *J. Am. Chem. Soc.* **2010**, *132*, 13978; g) Z. Wu, Y. Sun, Y. Tan, S. Yang, X. Feng, K. Müllen, *J. Am. Chem. Soc.* **2012**, *134*, 19532.

[8] D.-H. Ha, M. A. Islam, R. D. Robinson, *Nano Lett.* **2012**, *12*, 5122.

[9] V. Jayawarna, M. Ali, T. A. Jowitt, A. F. Miller, A. Saiani, J. E. Gough, R. V. Ulijn, *Adv. Mater.* **2006**, *18*, 611.

[10] J. Jiang, Y. Li, J. Liu, X. Huang, *Nanoscale* **2011**, *3*, 45.

[11] a) J. F. Ye, W. Liu, J. G. Cai, S. A. Chen, X. W. Zhao, H. H. Zhou, L. M. Qi, *J. Am. Chem. Soc.* **2011**, *133*, 933; b) V. Etacheri, J. E. Yourey, B. M. Bartlett, *ACS Nano* **2014**, *8*, 1491; c) Y. Ren, Z. Liu, F. Pourpoint, A. R. Armstrong, C. P. Grey, P. G. Bruce, *Angew. Chem. Int. Ed.* **2012**, *51*, 2164; *Angew. Chem.* **2012**, *124*, 2206; d) S.-T. Myung, M. Kikuchi, C. S. Yoon, H. Yashiro, S.-J. Kim, Y.-K. Sun, B. Scrosati, *Energy Environ. Sci.* **2013**, *6*, 2609; e) W. Li, J. Yang, Z. Wu, J. Wang, B. Li, S. Feng, Y. Deng, F. Zhang, D. Zhao, *J. Am. Chem. Soc.* **2012**, *134*, 11864.

[12] M. Doi, S. F. Edwards, *The Theory of Polymer Dynamics*, Oxford University Press, New York, **1986**.

[13] a) T. Kasuga, M. Hiramatsu, A. Hoson, T. Sekino, K. Niihara, *Langmuir* **1998**, *14*, 3160; b) H. Zhu, Y. Lan, X. Gao, S. P. Ringer, Z. Zheng, D. Song, J. Zhao, *J. Am. Chem. Soc.* **2005**, *127*, 6730.

[14] Y. Tang, Y. Zhang, J. Deng, J. Wei, H. L. Tam, B. K. Chandran, Z. Dong, Z. Chen, X. Chen, *Adv. Mater.* **2014**, DOI: 10.1002/adma.201402000.

[15] a) P. Liu, H. Zhang, H. Liu, Y. Wang, X. Yao, G. Zhu, S. Zhang, H. Zhao, *J. Am. Chem. Soc.* **2011**, *133*, 19032; b) Z. Jiang, Y. Tang, Q. Tay, Y. Zhang, O. I. Malyi, D. Wang, J. Deng, Y. Lai, H. Zhou, X. Chen, Z. Dong, Z. Chen, *Adv. Energy Mater.* **2013**, *3*, 1368.

[16] a) S. Brutti, V. Gentili, H. Menard, B. Scrosati, P. G. Bruce, *Adv. Energy Mater.* **2012**, *2*, 322; b) Y. G. Guo, Y. S. Hu, W. Sigle, J. Maier, *Adv. Mater.* **2007**, *19*, 2087.

[17] T. Fröschl, U. Hormann, P. Kubiak, G. Kucerova, M. Pfanzelt, C. K. Weiss, R. J. Behm, N. Husing, U. Kaiser, K. Landfester, M. Wohlfahrt-Mehrens, *Chem. Soc. Rev.* **2012**, *41*, 5313.

[18] M. Wagemaker, R. van de Krol, A. P. M. Kentgens, A. A. van Well, F. M. Mulder, *J. Am. Chem. Soc.* **2001**, *123*, 11454.

[19] a) M. Wagemaker, A. P. M. Kentgens, F. M. Mulder, *Nature* **2002**, *418*, 397; b) M. V. Koudriachova, N. M. Harrison, S. W. de Leeuw, *Solid State Ionics* **2004**, *175*, 829.

[20] a) S. Ding, J. S. Chen, D. Luan, F. Y. C. Boey, S. Madhavi, X. W. Lou, *Chem. Commun.* **2011**, *47*, 5780; b) N. Li, G. Zhou, R. Fang, F. Li, H.-M. Cheng, *Nanoscale* **2013**, *5*, 7780.

[21] D. Deng, M. G. Kim, J. Y. Lee, J. Cho, *Energy Environ. Sci.* **2009**, *2*, 818.

[22] a) Y. Li, X. Lv, J. Li, *Appl. Phys. Lett.* **2009**, *95*, 113102; b) J. Choi, S. Lee, J. Ha, T. Song, U. Paik, *Nanoscale* **2013**, *5*, 3230; c) H. Han, T. Song, E. K. Lee, A. Devadoss, Y. Jeon, J. Ha, Y. C. Chung, Y. M. Choi, Y. G. Jung, U. Paik, *ACS Nano* **2012**, *6*, 8308; d) D. P. Singh, A. George, R. V. Kumar, J. E. ten Elshof, M. Wagemaker, *J. Phys. Chem. C* **2013**, *117*, 19809.

[23] a) Y. Ren, L. J. Hardwick, P. G. Bruce, *Angew. Chem. Int. Ed.* **2010**, *49*, 2570; *Angew. Chem.* **2010**, *122*, 2624; b) K. Tang, Y. Yu, X. Mu, P. A. van Aken, J. Maier, *Electrochem. Commun.* **2013**, *28*, 54; c) B. Qiu, M. Xing, J. Zhang, *J. Am. Chem. Soc.* **2014**, *136*, 5852.

[24] a) Z. Chen, D. Zhang, X. Wang, X. Jia, F. Wei, H. Li, Y. Lu, *Adv. Mater.* **2012**, *24*, 2030; b) D. Wang, D. Choi, J. Li, Z. Yang, Z. Nie, R. Kou, D. Hu, C. Wang, L. V. Saraf, J. Zhang, I. A. Aksay, J. Liu, *ACS Nano* **2009**, *3*, 907; c) R. Mo, Z. Lei, K. Sun, D. Rooney, *Adv. Mater.* **2014**, *26*, 2084.

